NASA TECHNICAL NOTE

NASA TN D-4374

NASA TN D-4374

EXPERIMENTAL AND THEORETICAL INVESTIGATION OF THE ABLATIVE PERFORMANCE OF FIVE PHENOLIC-NYLON-BASED MATERIALS

by Allen G. McLain, Kenneth Sutton, and Gerald D. Walberg

Langley Research Center
Langley Station, Hampton, Va.

NATIONAL AERONAUTICS AND SPACE ADMINISTRATION • WASHINGTON, D. C. • APRIL 1968

NASA TN D-4374

EXPERIMENTAL AND THEORETICAL INVESTIGATION OF THE ABLATIVE PERFORMANCE OF FIVE PHENOLIC-NYLON-BASED MATERIALS

By Allen G. McLain, Kenneth Sutton,
and Gerald D. Walberg

Langley Research Center
Langley Station, Hampton, Va.

NATIONAL AERONAUTICS AND SPACE ADMINISTRATION

For sale by the Clearinghouse for Federal Scientific and Technical Information
Springfield, Virginia 22151 – CFSTI price $3.00

EXPERIMENTAL AND THEORETICAL INVESTIGATION OF THE ABLATIVE PERFORMANCE OF FIVE PHENOLIC-NYLON-BASED MATERIALS

By Allen G. McLain, Kenneth Sutton,
and Gerald D. Walberg
Langley Research Center

SUMMARY

Five composite ablation materials which contain various percentages of phenolic resin, powdered nylon, and silica (either as spheres or fibers) have been tested in the Langley 20-inch hypersonic arc-heated tunnel. The tests were carried out in air at a stream stagnation enthalpy of 4800 Btu/lbm (11.16 MJ/kg), a cold-wall aerodynamic heating rate of 119 Btu/ft^2-sec (1.35 MW/m^2), a stagnation pressure on the model surface of 0.066 atmosphere, and a free-stream Mach number of approximately 5. The data obtained from these tests have been used to evaluate the ablative performance of each of the materials and have been compared with theoretical predictions of char-recession rate and (for two of the materials) thermal response. During the tests, char removal was due primarily to oxidation and the char-recession rates were not significantly affected by either mechanical failure or SiO_2-C reactions. The addition of 12.5 percent (by weight) SiO_2 to the high-density materials produced a significant increase in both char integrity and char-virgin material interface strength but resulted in a decrease (approximately 20 percent) in thermal effectiveness. Reasonable agreement between measured and calculated char-recession rates was obtained by assuming chemical equilibrium at the char surface between the pyrolysis gases, the char, and the test stream, with CO as the primary reaction product. Reasonable agreement between measured and calculated thermal response could be obtained only when the char thermal conductivity was assumed to be approximately 1/3 of its measured value.

INTRODUCTION

A research program is presently being carried out at the Langley Research Center to define accurately the ablative response of promising heat-shield materials and to assess the ability of available theoretical analyses to predict this response. As a part of this program, five composite ablation materials which contain various percentages of phenolic resin, powdered nylon, and silica (either spheres or fibers) were selected for

testing in the Langley 20-inch hypersonic arc-heated tunnel. The test condition for this investigation was selected to yield information which would be applicable to portions of a lifting body where the phenolic-nylon-based materials might be applied for protection.

The group of five materials included three high-density ablators and two low-density ablators. One material in each density range has been extensively tested and is well characterized as to thermal properties. The high-density material, PN-1, has been tested extensively during the Stanford Research Institute Round Robin Ablation Program (see ref. 1), and the low-density material, PN-2, has been tested extensively at both the NASA Ames and Langley Research Centers. (See refs. 2 and 3.) The remaining materials have been altered slightly, by the inclusion of silica in the formulation, to assess whether the ablative abilities of the resulting materials are superior or inferior to the characterized formulation.

Theoretical predictions of the char recession for all the materials and of the thermal response for the two characterized materials were made and were compared with the experimental results. The results of the experimental and theoretical comparisons are presented in this paper.

SYMBOLS

The units used for the physical quantities defined in this paper are given both in the U.S. Customary Units and in the International System of Units (SI). (See ref. 4.)

c_p	specific heat at constant pressure, Btu/lbm-^{o}R (J/kg-^{o}C)
E	thermal effectiveness, Btu/lbm (J/kg)
k	measured thermal conductivity, Btu/ft-sec-^{o}R (W/m-^{o}K)
Δl	length change, ft (m)
l	length, ft (m)
M	Mach number
p	pressure, atm
$\dot{q}$	cold-wall heat-transfer rate, Btu/ft^2-sec (W/m^2)

R_B	body radius (fig. 1), ft (m)
s	distance from stagnation point along surface (fig. 1), ft (m)
T	temperature, ^{o}R (^{o}K)
t	time, sec
V	volume, ft^3 (m^3)
V'	corrected volume, ft^3 (m^3)
W	mass per unit area, lbm/ft^2 (kg/m^2)
$\dot{x}$	recession rate, in./sec (m/sec)
x,y,z	rectangular Cartesian coordinates
ϵ	emissivity
ρ	density based on original dimensions of char, lbm/ft^3 (kg/m^3)
ρ_o	density, lbm/ft^3 (kg/m^3)
τ	aerodynamic shear, lbf/ft^2 (N/m^2)

Subscripts:

c	char
l	local
t	stagnation point
ΔT	temperature rise
w	wall
o	initial

APPARATUS AND TESTS

Test Specimens

The composition and specific gravities of the char and of the uncharred materials are shown in table I. The char used in the specific-gravity determination was formed in a vacuum oven. A PN-1 material sample was not available for the char specific gravity determinations. The procedure used and the method for calculating specific gravity are described in the appendix. The specific gravities used in theoretical analyses performed in this paper are those obtained from the determination outlined in the appendix, with the exception of the PN-1 char which was obtained from reference 5. This method was used to insure that densities consistent with the actual ablation model moldings would be used in the theoretical analyses. The difference in specific gravity of the materials used in this test program and those listed in reference 5 was possibly caused by a slight difference in molding procedure. However, it is believed that since the same molding procedure was applied both for the materials used in this investigation and for those used in reference 5, the thermophysical properties reported in the reference are not grossly different and are thus suitable for use, subsequently, in the thermal analysis.

TABLE I.- MATERIAL COMPOSITION AND SPECIFIC GRAVITY AND CHAR SPECIFIC GRAVITIES AT 75° F (24° C)

Material	Composition	Percent total weight	Specific gravity			
			Virgin materials	Char		
				(a)	(b)	(c)
PN-1	Phenolic resin	50	1.240	----	----	----
	Nylon powder	50	[c]1.150	----	----	0.359
PN-2	Phenolic resin	25	0.707	0.243	0.234	----
	Nylon powder	50	-----	----	----	----
	Phenolic microspheres	25	[c].590	----	----	0.210
PN-4	Phenolic resin	15.8	-----	----	----	----
	Nylon powder	63.4	-----	----	----	----
	Phenolic microspheres	15.8	0.576	0.163	0.130	----
	Silica microspheres	5.0	-----	----	----	----
PNS-5	Phenolic resin	50	-----	----	----	----
	Nylon powder	45	1.233	0.401	0.337	----
	Silica fibers	5	-----	----	----	----
PNS-12	Phenolic resin	50	-----	----	----	----
	Nylon powder	37.5	1.280	0.510	0.347	----
	Silica fibers	12.5	-----	----	----	----

[a]Char containing SiO_2.

[b]Char with percentage SiO_2 subtracted.

[c]From TN D-2991 (ref. 5).

All test materials were subjected to a standard organic elemental analysis consisting of duplicate determination of C, O, H, N, and ash. The results of this analysis are listed in table II. This elemental composition is to be used subsequently in calculating theoretical char recession.

Each material was machined to the shape shown in figure 1(a). (The shape of the specimen was selected to provide a uniform heat-transfer rate across the surface.) A calorimeter plate of copper 0.0156 inch (0.0396 cm) in thickness is bonded to the back surface of the material. Three 30-gage thermocouple wires are spotwelded to the copper plate. The nose assembly is bonded to a cylindrical steel model holder protected with phenolic cork. A sectioned view of this construction is shown in figure 1(b).

Test Facility

The materials were tested in the Langley 20-inch hypersonic arc-heated tunnel, described in reference 6, adapted with a conical nozzle having a throat diameter of 0.538 inch (1.366 cm) and an exit diameter of 6.6 inches (16.75 cm). The flow is produced by heating the test medium (air in this study) with a magnetically rotated electric arc and expanding the heated gas through the conical nozzle to a Mach number of approximately 5. Figure 2 shows the 6.6-inch (16.75-cm) nozzle exit and an inserted test model. The nominal values for the stream parameters are presented in table III. Reference 6 also states various test conditions that may be obtained in this facility.

TABLE II.- ELEMENTAL ANALYSIS OF THE MATERIALS

(PERCENTAGES BY WEIGHT)

Material	Carbon	Hydrogen	Nitrogen	Oxygen	Ash	Total
PN-1	68.26	7.82	6.87	15.72	0.00	98.67
	68.07	7.89	6.72	15.91	.29	98.88
PN-2	65.59	7.78	7.25	17.08	1.06	98.76
	65.57	7.68	7.05	17.09	1.15	98.54
PN-4	61.21	7.86	7.89	15.80	4.97	97.73
	61.30	7.87	7.95	15.75	5.22	98.06
PNS-5	64.62	7.41	7.10	14.53	4.72	98.38
	64.47	7.70	7.13	14.39	4.92	98.61
PNS-12	60.08	6.67	7.11	13.28	12.03	99.17
	60.18	6.86	7.05	13.25	12.28	99.62

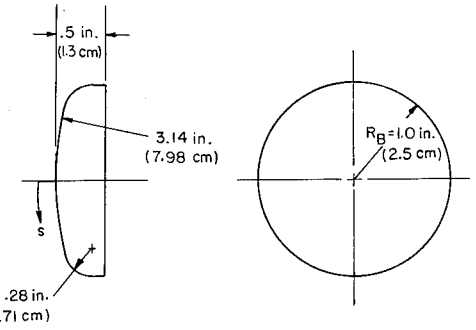

(a) Shape of material test specimen.

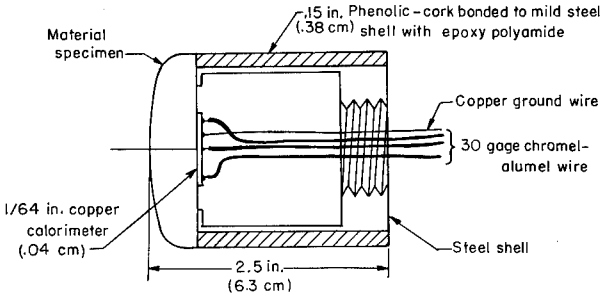

(b) Material specimen and thermocouple assembly.

Figure 1.- Ablation model construction.

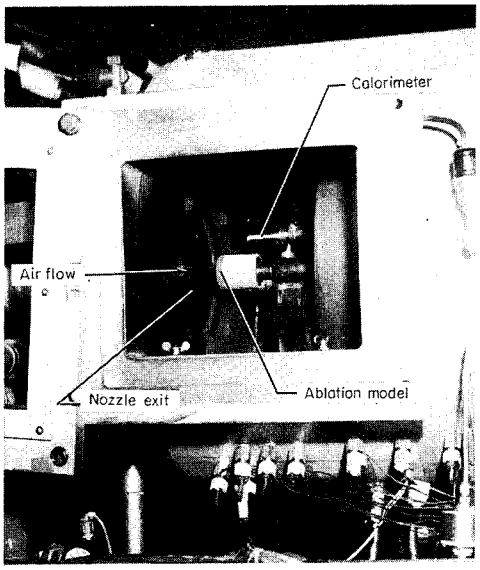

L-67-8705
Figure 2.- Ablation model and calorimeter in test section.

TABLE III.- NOMINAL (AVERAGE) TEST CONDITIONS

Free-stream Mach number (calculated, equilibrium flow assumed)	5
Stagnation enthalpy	4800 Btu/lb (11.16 MJ/kg)
Stagnation pressure behind a normal shock	0.066 atm
Stagnation heat-transfer rate (2-in.-diam. model, fig. 4)	119.0 Btu/ft^2-sec (1.35 MW/m^2)
Stream composition	Air

Instrumentation

Facility instrumentation.- The tunnel is equipped with high-speed motion-picture cameras, a photographic optical pyrometer (ref. 7), and recording oscillographs. All time-dependent measurements, such as millivolt outputs from pressure transducers and thermocouples, are recorded on film or photographic paper. The arrangement of the photographic equipment with respect to location of the test material is shown in figure 3. As can be seen in figure 3 the photographic optical pyrometer is actually viewing the model profile. When this instrument is focused on a plane subject, the accuracy is ±3 percent of the actual value.

Heat-transfer model.- To determine the heat-transfer rate to the model, a thin-wall calorimeter was used. The calorimeter is pictured and illustrated in figure 4. The shape is the same as that for the test specimens. The calorimeter is made of stainless steel with a wall thickness of 0.05 inch (0.127 cm). Chromel-alumel thermocouples are distributed about the nose and sidewalls to monitor the temperature rise of the steel. The following relation

$$\dot{q} = \rho c_p l \frac{\Delta T}{\Delta t}$$

is used to compute the heat-transfer rate at the selected points about the model.

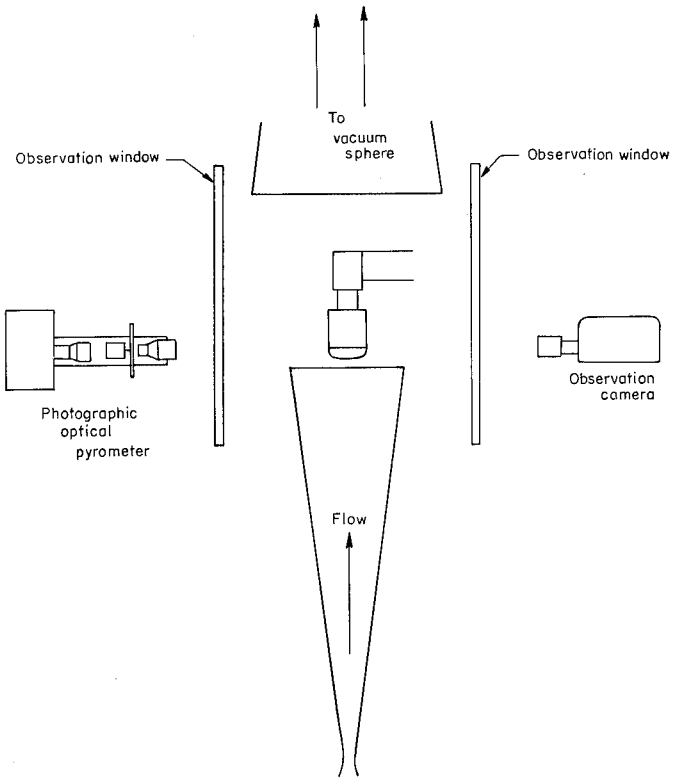

Figure 3.- Arrangement of equipment and ablation model in tunnel.

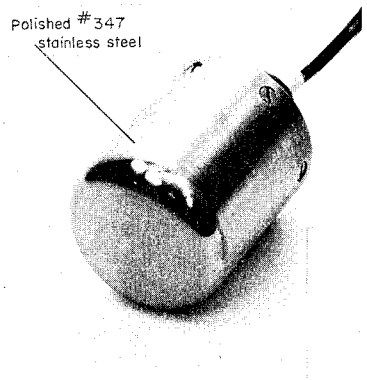

L-67-8706

(a) Photograph of slope-type calorimeter.

Thermocouple no.	s/R_B
①	0
②	.375
③	.800
④	1.168
⑤	1.548
⑥	2.048
⑦	2.548

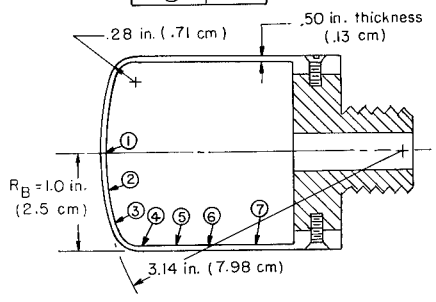

(b) Diagram illustrating thermocouple placement.

Figure 4.- Heat-transfer distribution model.

Pressure model.- The model used to determine the pressure distribution at the test condition is illustrated in figure 5. The probe was machined to the specific shape of the test specimens. Orifices were placed across the nose and along the sidewalls. Strain-gage pressure transducers were used to convert pressure into electrical impulses suitable for recording.

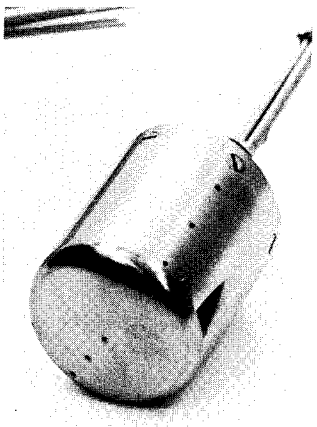

L-67-8707
(a) Photograph of pressure probe illustrating orifice.

Orifice no.	s/R_B
①	0
②	.40
③	.80
④	1.00
⑤	1.168
⑥	1.868
⑦	2.568

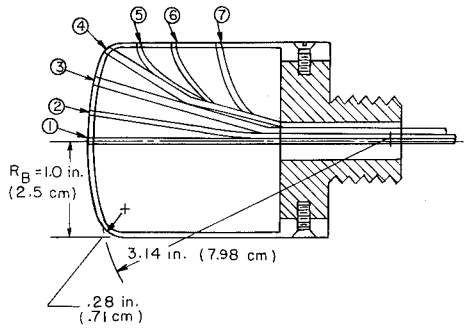

(b) Diagram of orifice placement.

Figure 5.- Pressure distribution model.

Test Procedure

The procedure followed in testing the ablation materials was planned to ensure the acquisition of consistent and repeatable data. The power input and chamber pressure for the arc-heated tunnel were regulated carefully in order to maintain the same values throughout the entire test series. The stepwise ablation test procedure was as follows:

(1) The material test specimen was installed inside the tunnel and the test chamber was evacuated. The model was exposed to a vacuum for about 30 minutes.

(2) The tunnel was started, and time (25 sec) was allowed for transient conditions to subside.

(3) A thin-wall calorimeter was then inserted into the test stream for a short period of time (1 sec) and withdrawn.

(4) The material specimen was exposed to the test stream for the desired period of time. It was then retracted and allowed to cool in the low pressure environment.

(5) The calorimeter was inserted into the stream again and then the tunnel was shut down.

(6) The material specimen was then extracted from the tunnel for further observation.

The material recession rate was determined from data obtained by testing five specimens for successively longer exposures, as well as from the motion-picture film. The exposure times ranged from 30 to 150 seconds in equal increments. The measurements were taken from the sectioned specimens.

Determination of Stream Conditions

Pressure and heat-transfer-rate distribution models were tested in conjunction with the ablation models to determine the existing test conditions. The enthalpy, pressure, and heat-transfer-rate determinations resulting from this phase of the investigation are presented in the following sections.

Enthalpy determination.- The enthalpy of the test stream was determined by computing a heat balance of the arc jet. This computation was arrived at from data on the known total power input to the arc and the total heat removed by cooling and conduction. By this method, an enthalpy of 4800 Btu/lbm (11.16 MJ/kg) was calculated. This value represents an average of the entire test series. Individual test enthalpies varied by ±12.0 percent from this average.

Pressure determination.- A stagnation-point pressure of 0.066 atmosphere was measured. The experimentally determined nondimensional pressure distribution about the model is shown in figure 6. The symbols represent the experimental data obtained in this study, whereas the solid curve represents experimental data obtained in a different facility on a similar nose shape (ref. 8). The shapes of the pressure distribution curves are similar. The difference in magnitude of the pressure ratios beyond an s/R_B of 1.2 results from a different side-wall geometry. It should be noted that the test

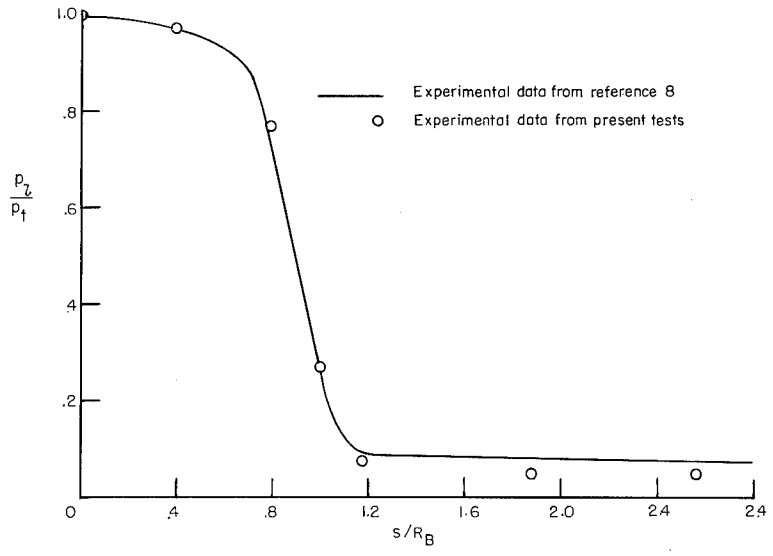

Figure 6.- Nondimensional pressure distribution about the model.

material only extends to an s/R_B value of 1.30 and that within this range the measured pressure distribution is in good agreement.

Heat-transfer-rate determination.- The stagnation-point heat-transfer rate for each test was selected as an average of the heat-transfer rates measured before and after the material ablation test. A mean stagnation-point heat-transfer rate over the entire series of tests was found to be 119 Btu/ft^2-sec (1.35 MW/m^2). Individual stagnation-point heat-transfer rates varied by ±13 percent from the mean. The standard deviation in heat-transfer rate over the entire series was only 7 percent of the mean.

The measured pressure distribution and average total enthalpy were used in an isentropic expansion to compute the velocity distribution about the body. After the velocity distribution about the specific body shape was specified, the heat-transfer rates and shears were evaluated by the similar solution of the boundary-layer equations for real air. (For example, see refs. 9 and 10.) This approach yielded a heat-transfer rate of 118 Btu/ft^2-sec (1.34 MW/m^2) for the stagnation point. The nondimensional heat-transfer-rate distribution determined by this method is shown in figure 7 as the solid curve. The symbols illustrate the distribution determined by the thin-wall calorimeter in this experimental investigation. The variation of the experimental data over the entire series of tests is illustrated by use of the bars. This spread represents good agreement between the analytically determined and measured heat-transfer distributions except for the peak expected at the corner, which was believed to have been obscured experimentally through conduction. Reference 8 indicated a similar loss of the expected peak.

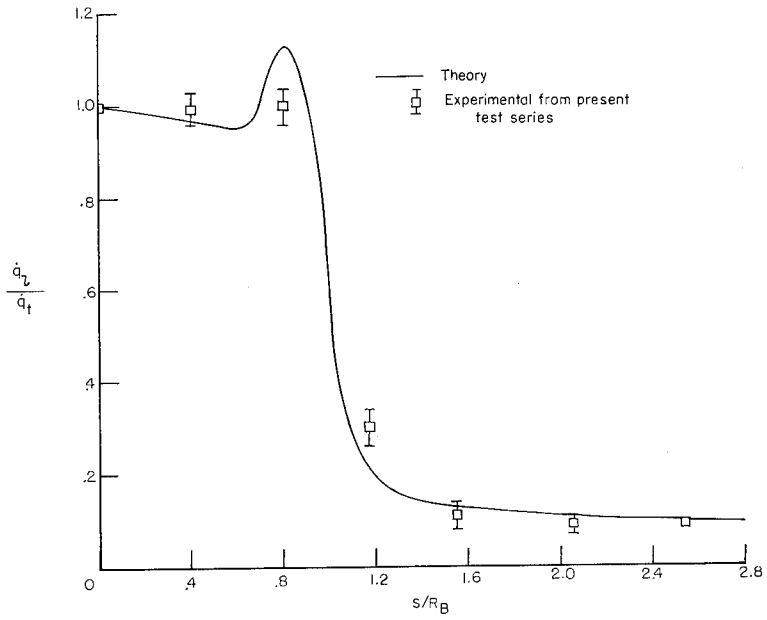

Figure 7.- Comparison of experimental and theoretical heat-transfer-rate distributions about the model.

The shear variation about the body is shown in figure 8. The peak value of shear was approximately 6 lbf/ft^2 (287.3 N/m^2) located at an s/R_B of 0.95. This value of shear is below that expected to cause mechanical failure of the char of presently used ablation materials.

RESULTS AND DISCUSSION

Determination of Material Performance

The performance of the five phenolic-nylon-based materials during exposure to the test stream is based on observed behavior of the charred surface during the tests, measured surface temperatures, recession of char and uncharred material, and back-surface temperature rise. Each of these criterion for judging a material's performance is discussed in the following sections.

Surface behavior.- From the photographic pyrometer and motion-picture films, the charred surfaces were noted to form a network of cracks from the outset of the tests. The cracks appeared less extensive in the models containing silica. Bubbles which appeared to be molten silica were observed to form at an s/R_B of approximately 1 for the specimen containing silica. The appearance of the material's surface after the longest exposure may be observed from the photographs in figure 9. The series of photographs in figure 9(a) shows the effects of silica addition to the high-density materials. As can be seen, the surface becomes progressively less cracked with increased addition of silica. In figure 9(b) the effect of silica addition is not quite so clear; however, the surface appears somewhat smoother for the material containing silica, PN-4. (The defect in the PN-4 surface was caused by handling after the test.)

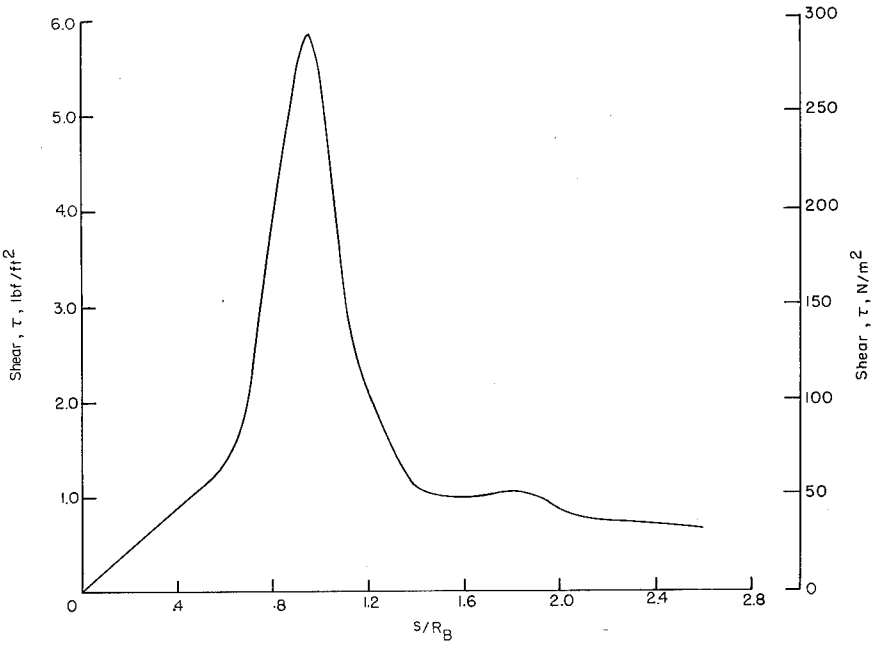

Figure 8.- Theoretical shear distribution about the model.

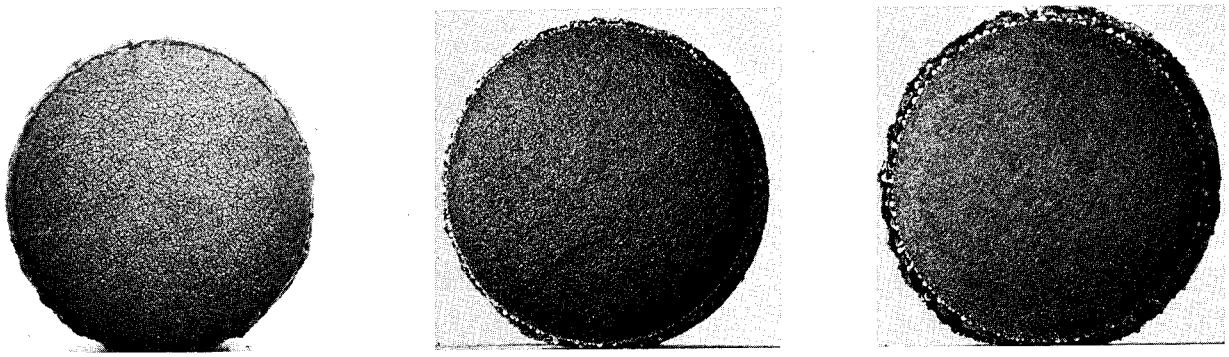

PN-1 (No silica)
150 - second exposure time

PNS-5 (5 percent silica)
150- second exposure time

PNS-12 (12.5 percent silica)
150-second exposure time

(a) High-density materials.

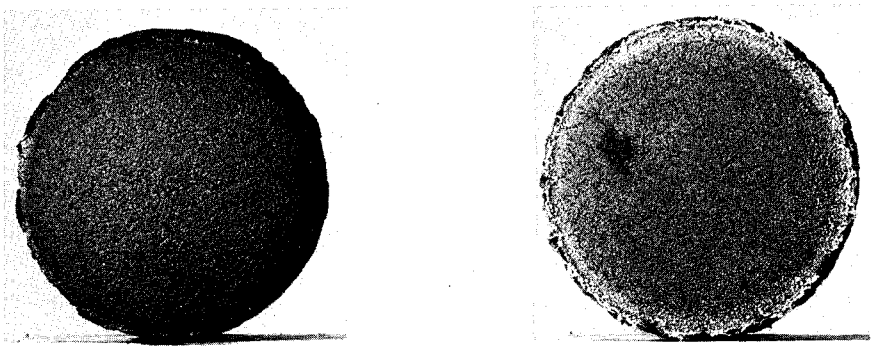

PN-2 (No silica)
150 - second exposure time

PN-4 (5 percent silica)
120- second exposure time

(b) Low-density materials. L-67-8708

Figure 9.- Charred surface of the phenolic-nylon-based materials illustrating the effect of silica addition.

The surface temperature of each material was recorded by means of a photographic optical pyrometer. Figure 3 shows the arrangement of this camera and the model. It is evident from the illustration that the camera was not alined for viewing the stagnation area of the model. The surface temperatures recorded from viewing the profile of the model, however, are believed to be representative of the actual stagnation-point surface temperature. This observation is further supported by the fact that when the surface temperature was read from the photographic optical pyrometer film to an s/R_B of 0.59 for a typical material, PN-2, the maximum variation from the value taken at the stagnation point was less than 5 percent.

When the surface temperatures measured during each of the successively longer tests of a given material were overlaid, it was found that they agreed and exhibited a maximum deviation from the mean curve of ±7 percent. Accordingly, the variation of surface temperature with time for a given material was determined by fitting a fourth-

degree polynomial (least-squares fit) to a composite plot of all of the surface temperature data for that material. As an example, the surface-temperature data of PN-2 (which exhibited the greatest deviation from a mean curve) are presented in figure 10.

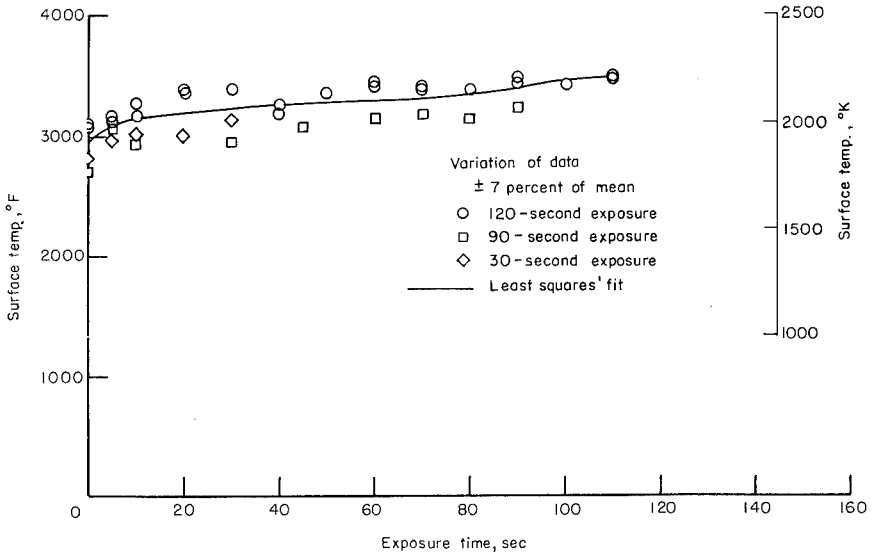

Figure 10.- Surface temperature of PN-2 with least squares curve.

The surface-temperature time histories obtained in this manner for each of the five materials tested are presented in figure 11. The temperatures presented in figures 10 and 11 are brightness temperatures (emissivity of 1.0).

Char character.- The difference in char character between materials containing silica and those not containing silica is readily apparent from the profile photographs of figure 12. The PN-1 specimen, which did not contain silica, formed a very weak, columnar-type char with a weak connection to the uncharred material.

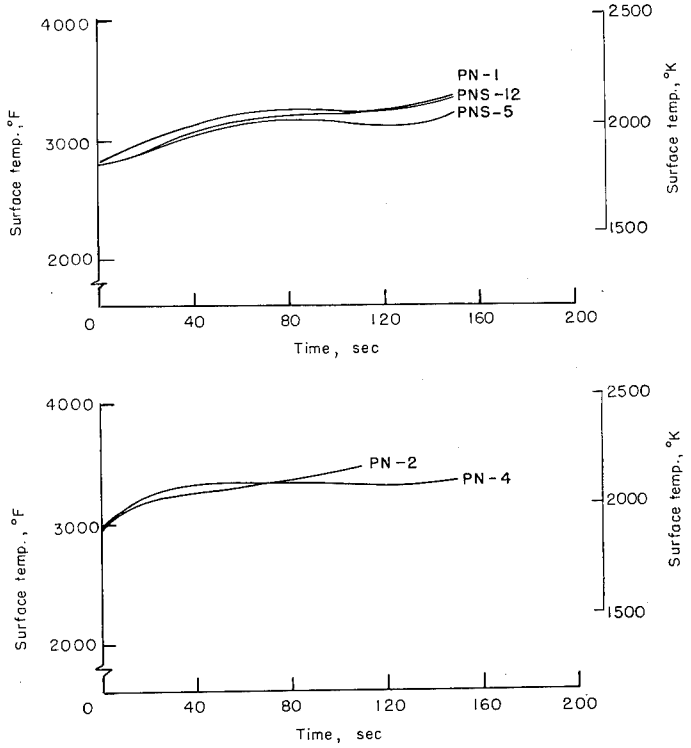

Figure 11.- Surface brightness temperature histories.

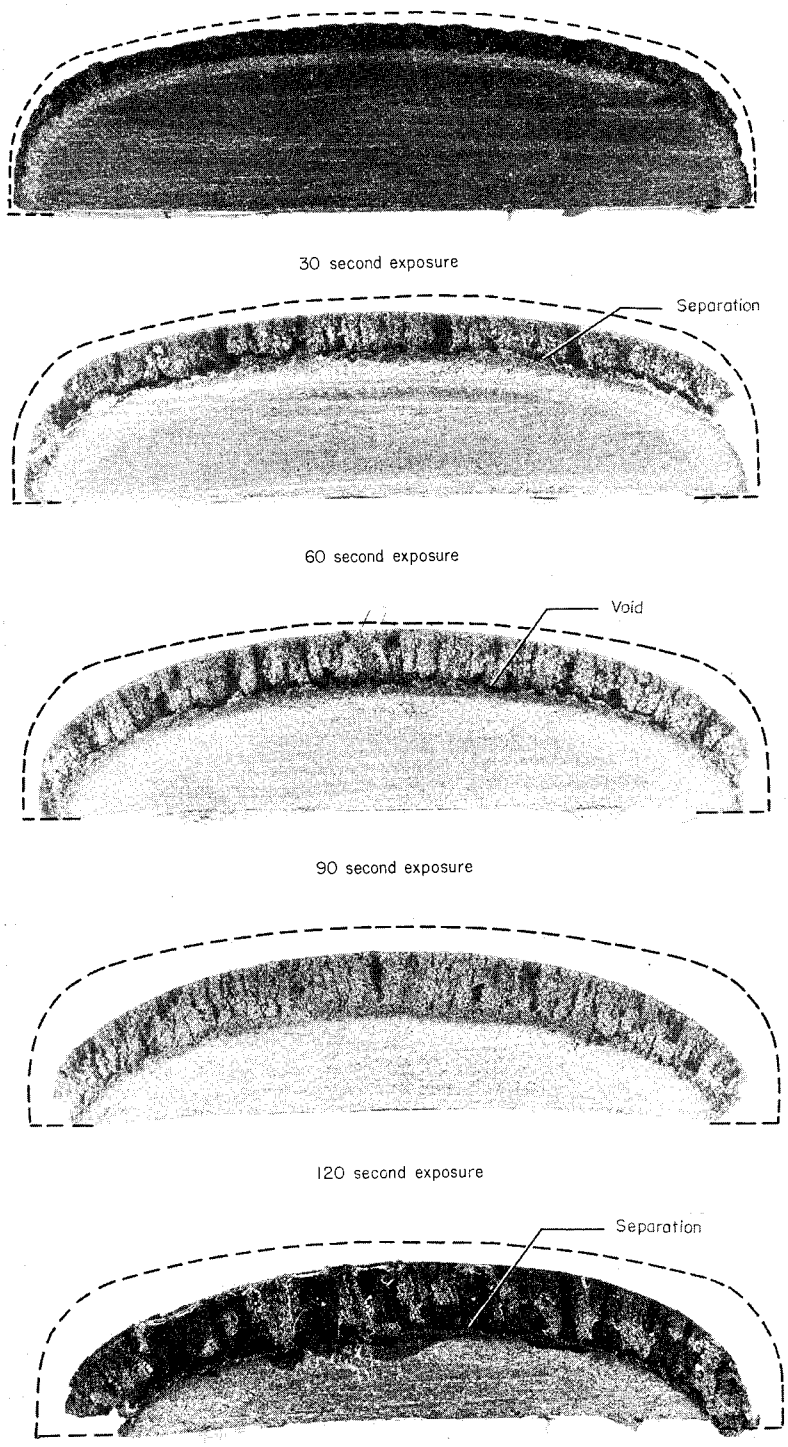

(a) PN-1. L-67-8709

Figure 12.- Sectioned views of specimens depicting char and virgin material changes for successively longer exposure times.

30 second exposure

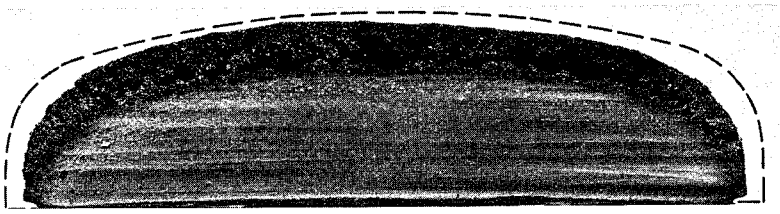

60 second exposure

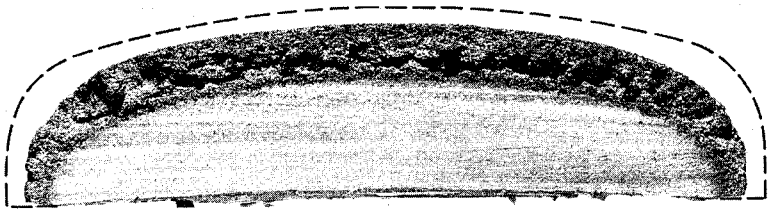

90 second exposure

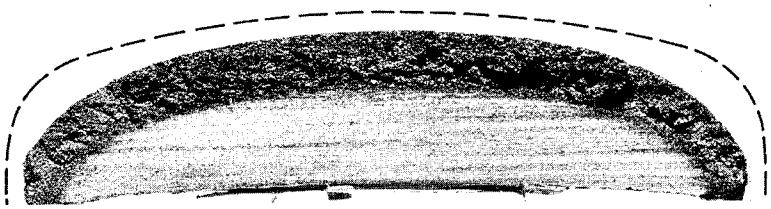

120 second exposure

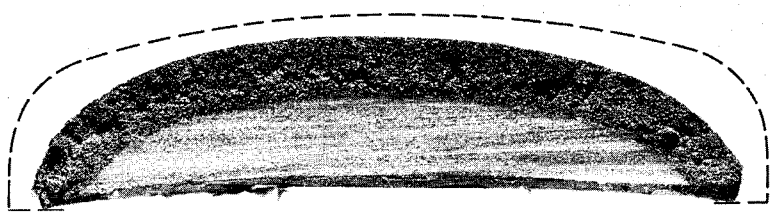

150 second exposure

(b) PNS-5. L-67-8710

Figure 12.- Continued.

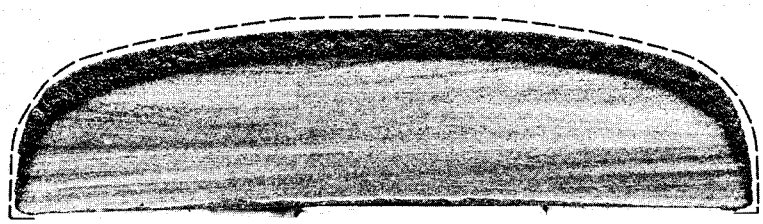

30 second exposure

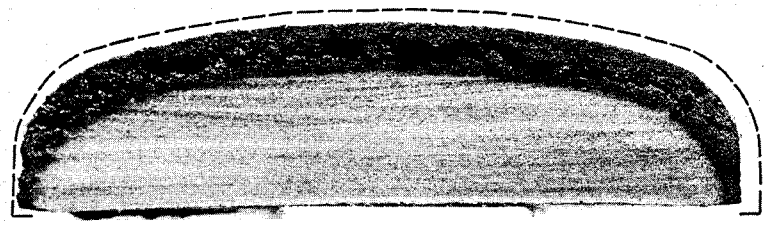

60 second exposure

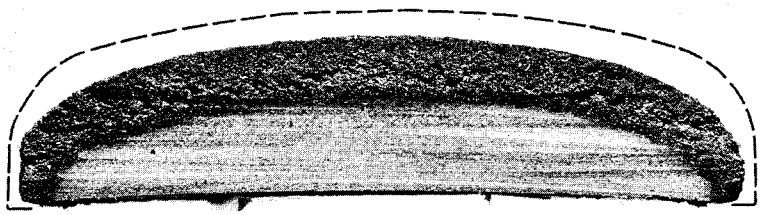

90 second exposure

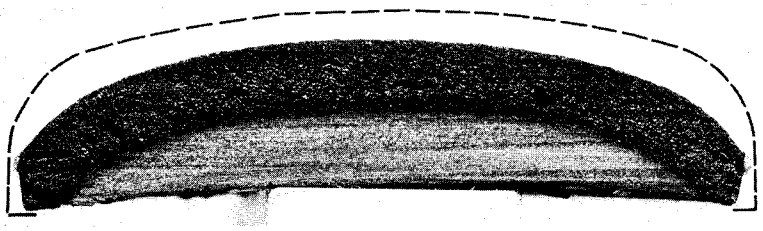

120 second exposure

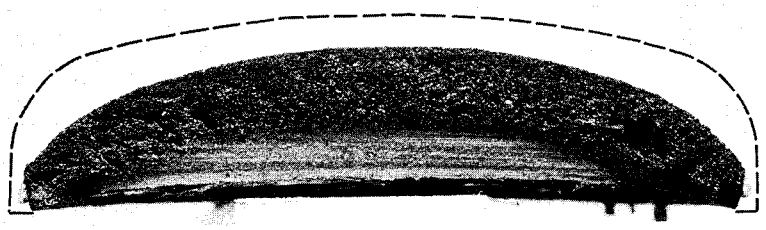

150 second exposure

(c) PNS-12. L-67-8711

Figure 12.- Continued.

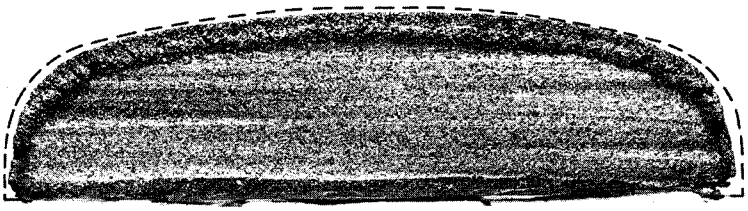

30 second exposure

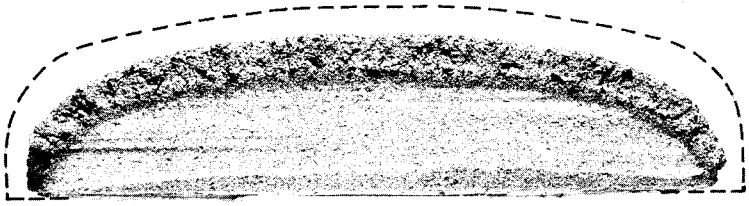

60 second exposure

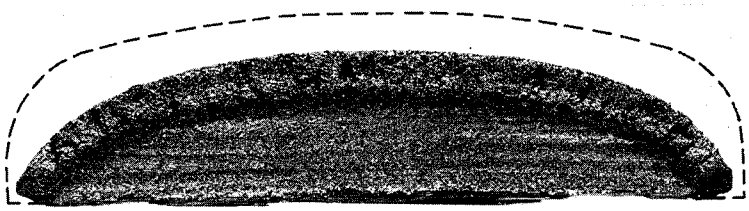

90 second exposure

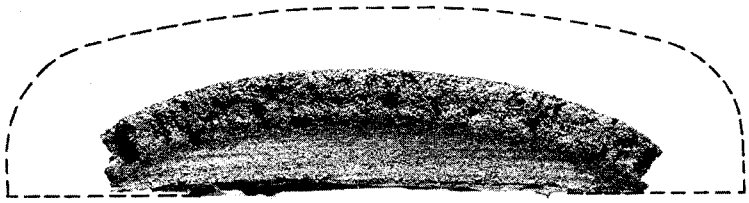

120 second exposure

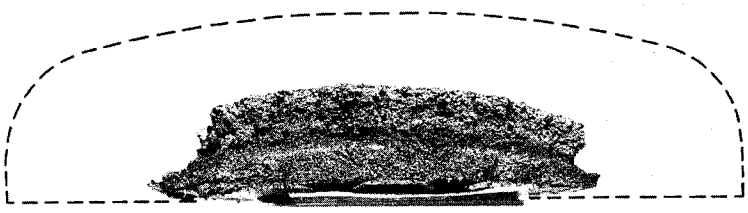

150 second exposure

(d) PN-2. L-67-8712

Figure 12.- Continued.

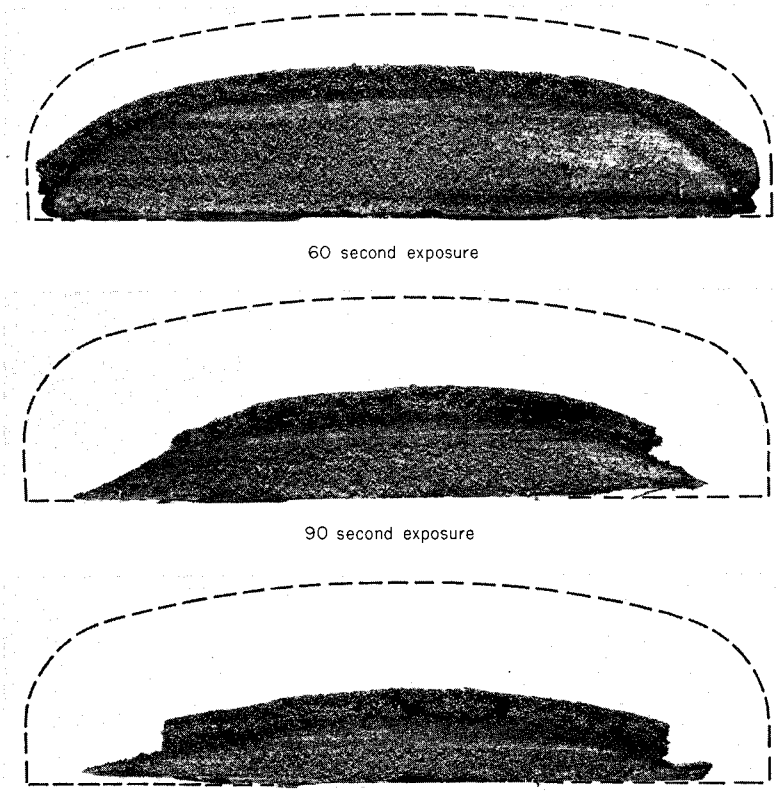

(e) PN-4. L-67-8713

Figure 12.- Concluded.

As shown in figure 12, the char for PN-1 models exposed to the test stream for 60 and 150 seconds separated completely from the uncharred material. The model tested for 90 seconds exhibited a void just above the pyrolysis interface, but did not separate on sectioning. Models PNS-5 and PNS-12, however, each formed a strong char, without an apparent columnar structure. The low-density materials formed very similar chars, and were not apparently columnar in form.

Material recession.- The five phenolic-nylon-based materials receded smoothly with no evidence of mechanical char failure. The irregularities in the chars shown in figure 12 resulted from the sectioning process. Sectioned model photographs shown in this figure illustrate the relative smoothness of the char surface for successively longer test times. The small amount of shape change and the uniform char-layer thickness indicates the extent to which a uniform heat-transfer rate and oxygen flux across the model nose was obtained. The original model outlines shown in figure 12 are intended only to give an idea of the relative shape change of the front surface and should not be misinterpreted as indicative of model recession.

The recession histories for the five phenolic-nylon-based materials are shown in figure 13. These plots were obtained by measuring the sectioned specimens after successively longer exposure times. The data presented in this figure show that char thicknesses for exposure times greater than 60 seconds are essentially constant. The ablative process is thus inferred to approach a steady state at exposures beyond this time.

Char-recession rates are presented in table IV. The range of recession-rate data was included in order to illustrate the possiblity of fairing many different straight lines through the char surface data points. The two values represent minimum and maximum slopes of fairings through the char-surface points in figure 13.

TABLE IV.- CHAR-RECESSION RATES

Material	Motion picture		Measured after tests	
	$\dot{x}$		$\dot{x}$	
	in./sec	mm/sec	in./sec	mm/sec
PN-1	7.05×10^{-4}	0.0179	5.6 to 8.0×10^{-4}	0.0142 to 0.0203
PN-2	14.6	.0371	15.28 to 20.0	.0388 to .0508
PN-4	22.4	.0569	22.2 to 22.5	.0564 to .0572
PNS-5	5.28	.0134	7.58 to 10.5	.0193 to .0267
PNS-12	9.05	.0230	9.33 to 11.5	.0237 to .0292

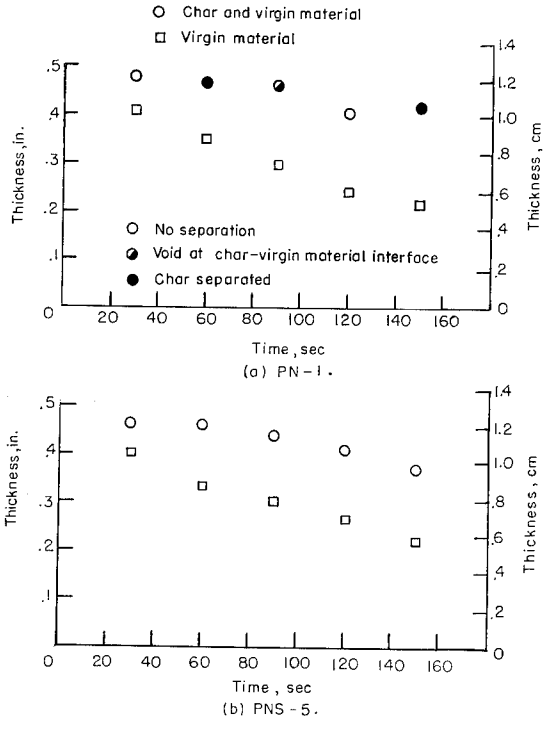

Figure 13.- Recession histories of ablation materials determined from sectioned models.

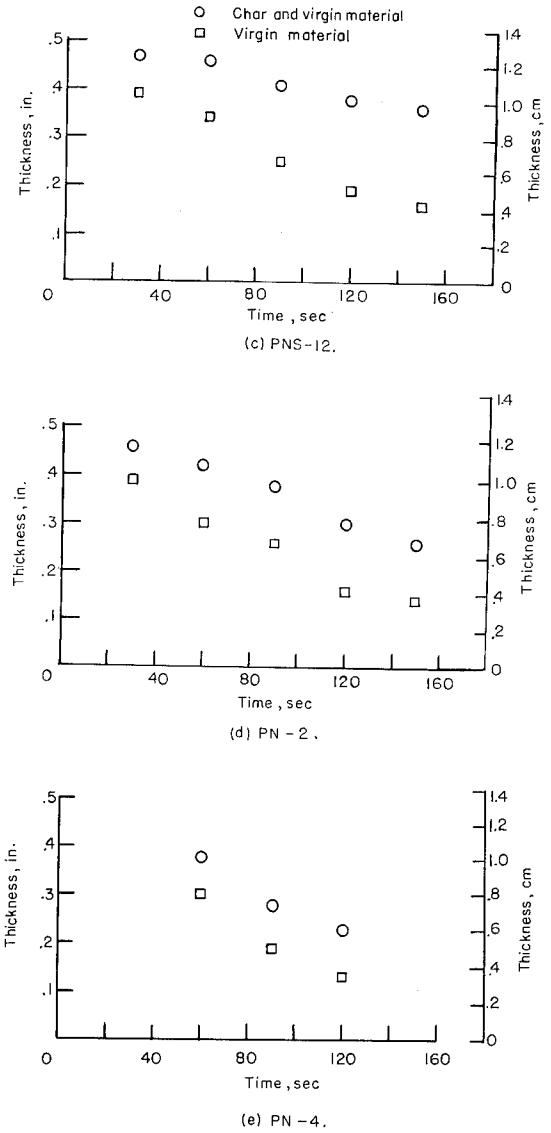

Figure 13.- Concluded.

The char-surface-recession rates were also taken from the motion-picture film of the longest tests. The material recession history determined for PN-2 from the motion-picture film is shown in figure 14. The specimen appeared to expand over the first few seconds and then to exhibit a linear recession. The linear portion of the curve was used to determine a recession rate for the char surface. The rates for the five materials are presented in table IV.

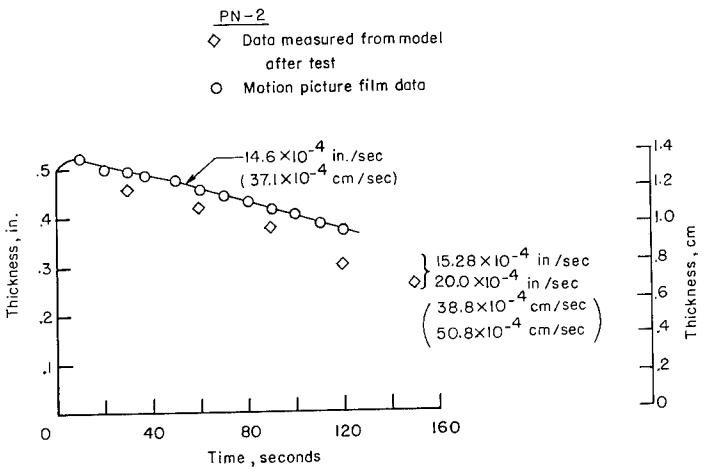

Figure 14.- Typical front surface recession history as recorded by motion-picture camera.

The apparent difference in actual final length and the final length obtained from the film is attributed to overexposure of the film caused by the extreme brightness of the surface. The linear portion of the curve (fig. 14) corresponds to the constant surface-temperature portion and therefore the same degree of overexposure. The initial portion of the recession curve, where an apparent expansion is indicated, corresponds to the period where model temperature is rising and overexposure is occurring. (Evidence that has been gathered through use of a rotating filter illustrates that as the exposure is corrected, the apparent model length is reduced.)

Thermal effectiveness.- Although material erosion is very important in judging the performance of an ablative material, the insulation afforded by the material must also be examined. The thermal effectiveness, which is defined by the relation:

$$E = \frac{\dot{q}t_{\Delta T}}{W}$$

has been used by several investigators as a measure of the insulation quality of a material (refs. 3 and 11). It should be noted that E is useful only in comparing materials at a given test condition.

Thermal effectiveness is calculated by obtaining the time for a specified back surface temperature rise $t_{\Delta T}$ from a temperature history plot. Such a plot is shown in figure 15 for a typical test material (PN-2 in this case). The solid curve represents a least-squares fit of the temperature-rise data for five different exposure times. A similar curve was plotted for each material and represents a nominal temperature rise

at the back surface for the specific test condition. The effectiveness of each of the materials was calculated and plotted against temperature rise for the entire range of temperatures as shown in figure 16.

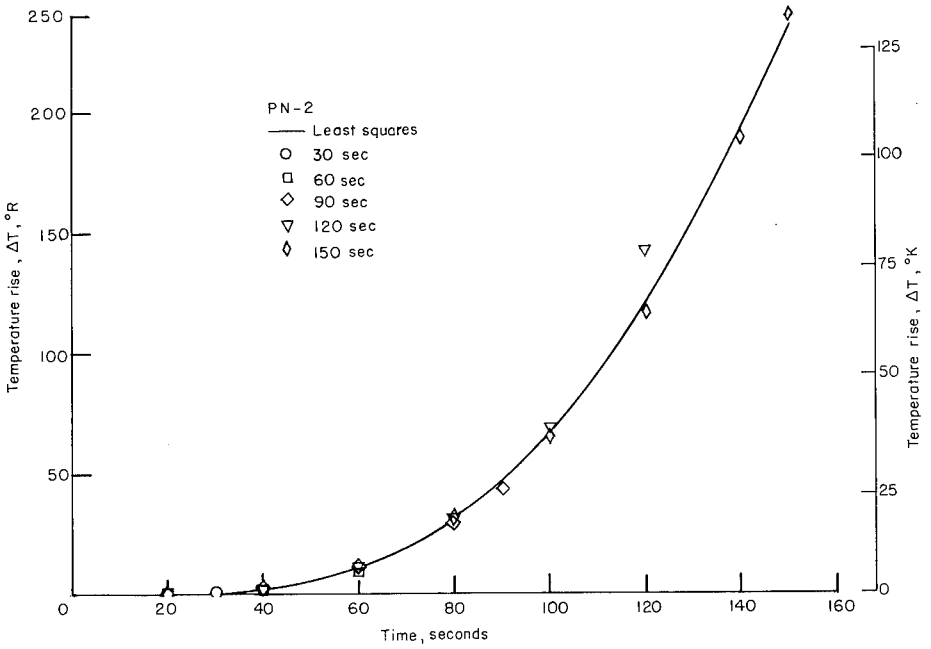

Figure 15.- Typical back surface temperature rise curve.

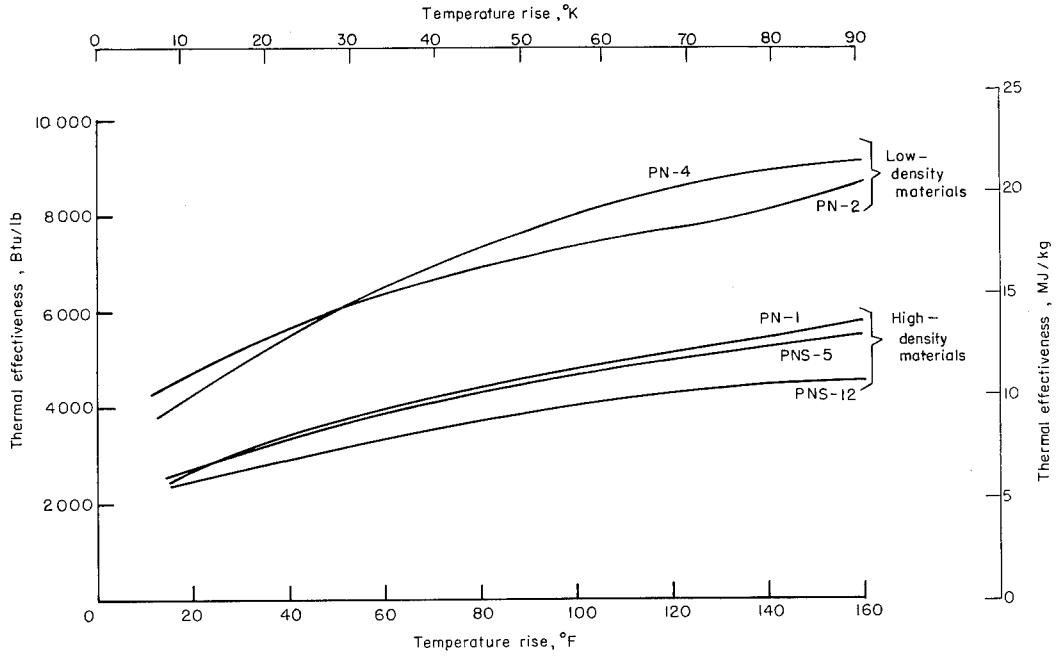

Figure 16.- Variation of thermal effectiveness with temperature rise.

Since the unit weight was not the same for the high- and low-density materials, a direct comparison between the two groups of materials is not possible. However, in reference 4, the thermal effectiveness was shown to increase with increasing unit weight. From consideration of this result in relation to the thermal-effectiveness value in figure 16, it is obvious that the low-density materials would exhibit even higher values of thermal effectiveness, if their unit weights were increased until equivalent to the unit weights of the high-density materials. The addition of 5 percent silica to the high-density material resulted in a slight reduction of effectiveness from the basic material without silica. An addition of 12.5 percent of silica results in a considerable reduction of thermal effectiveness. Since (as discussed in a subsequent section of this paper) SiO_2-C reactions did not contribute significantly to char removal during the present tests, it appears that this decrease in effectiveness was caused by changes in material properties (for example, thermal conductivity) associated with the increasing SiO_2 content of the materials. It should be recalled, however, that addition of silica improved the char-retention properties of the material.

Comparison with Ablation Theory

Predictions of char oxidation and thermal response (for two of the materials tested in this investigation) have been made by utilizing currently available theoretical approaches. These predictions have been compared with the experimental results obtained from this test series. The results of this comparison are discussed in the following sections.

Char-oxidation rates.- As mentioned previously, no mechanical char failure was observed during the tests in this investigation. Hence, the char removal may be assumed to be due entirely to chemical reactions between the char, the ablative pyrolysis gases, and the test stream.

The oxidation of a carbonaceous material (such as a char layer) is characterized at low surface temperatures by a kinetically controlled regime (in which oxidation rates are strongly dependent on surface temperature) and at high surface temperatures by a transport controlled regime (in which oxidation rates are dependent on the rate at which oxygen is delivered to the reacting surface and are virtually independent of surface temperature) and at temperatures between by a transition regime. These two reaction regimes have been discussed at length in the literature. (See, for instance, refs. 12 to 14.)

The first step to be taken in analyzing the char-recession rates obtained in the present investigation is to decide whether the observed oxidation was in the kinetically controlled, transport controlled, or transition regime. Although few data on the kinetics

of actual char layers are available, a reasonable assessment of the problem can be obtained by considering the behavior of graphite, for which there is an ample literature (see refs. 12 to 19) at the test conditions of the present investigation. Scala (refs. 12 and 17) has surveyed the literature and has defined "fast" and "slow" kinetics which bracket the bulk of the kinetic data for graphite. In reference 12, Scala has presented an analysis of graphite combustion which shows that, for the present test conditions, namely, T_w between 3400° R (1890° K) and 3900° R (2170° K); $p_w = 0.066$ atm, the stagnation-point oxidation of graphite would be completely transport controlled, even if the "slow" kinetics were used.

In recent years considerable attention has been directed toward the study of silica-carbon reactions as a possible char-removal mechanism (refs. 20 and 21). Since three of the materials tested in this investigation contained significant amounts of silica, the possibility of SiO_2-C reactions during the present tests is of interest. The char oxidation analysis presented in reference 22 provides a relation between virgin-plastic composition and char-recession rates and, hence, is well suited to studying the effects of SiO_2 additives. In essence, the addition of SiO_2 to the virgin plastic provides additional oxygen which could conceivably react with and remove the char. To assess the possible effect of SiO_2 on the present test results, calculations of char-recession rates were made by using the analysis presented in reference 22. All the oxygen present in the SiO_2 was assumed to react with the char as follows:

$$2C(s) + SiO_2 \rightarrow 2CO + Si$$

This approach yields the maximum effect on the char-recession rates. The recession rates calculated in this manner are presented in table V. The maximum possible effect of SiO_2-C reactions is comparable to or smaller than the uncertainty in the experimental results listed in table IV. Hence, the present experimental results do not possess sufficient accuracy to show the presence or absence of SiO_2-C reactions. The magnitudes of the possible changes in char-recession rate due to SiO_2-C reactions do, however, indicate that even if SiO_2-C reactions occurred in the present tests, they did not significantly affect the test results.

TABLE V.- PERCENT VARIATION IN CHAR RECESSION WITH MAXIMUM SiO_2-C REACTION

Material	$\dot{x}_c$ (inert SiO_2)		$\dot{x}_c$ (reactive SiO_2)		Percent change in $\dot{x}_c$ because of reactive SiO_2
	in./sec	mm/sec	in./sec	mm/sec	
PN-1	9.32×10^{-4}	0.0237	9.32×10^{-4}	0.0237	0
PN-2	17.05	.0433	17.05	.0433	0
PN-4	22.20	.0564	23.00	.0584	3.60
PNS-5	9.75	.0248	10.10	.0257	3.60
PNS-12	9.95	.0253	10.76	.0273	8.15

Two basically different approaches to the calculation of transport-controlled char-oxidation rates have been presented in the literature. The first approach (typified by ref. 23) treats the pyrolysis products as being chemically inert and assumes that the only reactions

occurring at the char surface are between the oxygen diffusing through the boundary layer and the char. This approach is consistent with the assumption that either CO or CO_2 is the primary reaction product, but most investigators have assumed the primary reaction product to be CO. The second approach (typified by ref. 22) assumes local chemical equilibrium (both heterogeneous and homogeneous) at the char surface and thereby accounts for reactions between the pyrolysis gases, the test stream, and the char. This second approach results in CO as the primary oxidation product.

Transport-controlled char-oxidation rates have been calculated for the present test conditions by two techniques. These two techniques are (with primary reaction product assumed to be CO):

(1) Analysis of reference 23 (pyrolysis gases inert)

(2) Analysis of reference 22 (pyrolysis gases reactive)

The results of these calculations are compared with the present experimental results in figure 17. In these calculations, the average stream properties (table III), the elemental analysis of the materials (table II), the virgin-plastic densities measured in the present investigation (table I), and the char densities with the SiO_2 removed (table I) were used for all the materials except PN-1. In the case of PN-1, the same procedure was followed with the exception that the char density from reference 5 was used. In all these calculations, the assumption of steady state ablation has been made and blowing coefficients were calculated by the method of reference 22. The bars attached to the symbols in figure 17 indicate the uncertainty in the experimental results which has been discussed previously. From figure 17 it is seen that the oxidation rates calculated by technique (1) are significantly higher than the experimentally measured rates. On the other hand, rates calculated by technique (2) are in reasonable agreement with the experimental results.

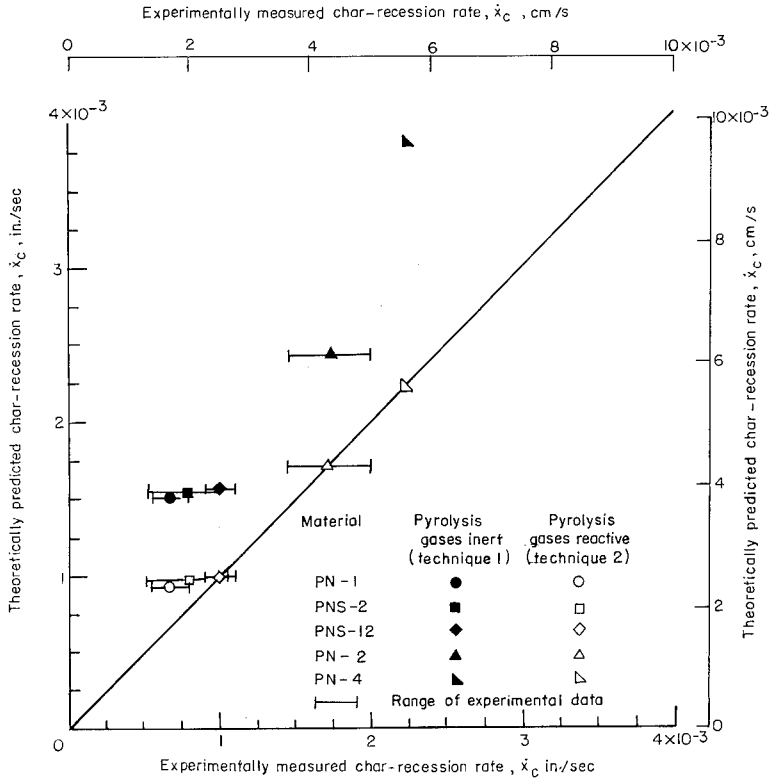

Figure 17.- Calculated and measured char-recession rates.

Thermal response.- The thermal responses of two of the phenolic-nylon-based materials, PN-1 and PN-2, were predicted by using the numerical analysis computer program described in reference 24. These two materials were selected for the comparison because they are representative of high- and low-density composite materials, and the necessary thermophysical properties have been measured and reported in reference 5. This reference also contains measured thermophysical properties for the chars formed by the decomposition of the two materials.

Before the analysis was undertaken, the decision was made that only char thermophysical properties would be altered, if any alteration were necessary, to obtain a close comparison between experimental and computed results. Questions regarding the reliability of measured char thermophysical properties, specifically the char thermal conductivity, have been expressed by several experimenters. (See refs. 25 and 26, for instance.) For all computed cases, the surface recession was forced to follow the experimental recession data. This restriction was imposed to ensure that only the effect of thermophysical property alterations would be observed.

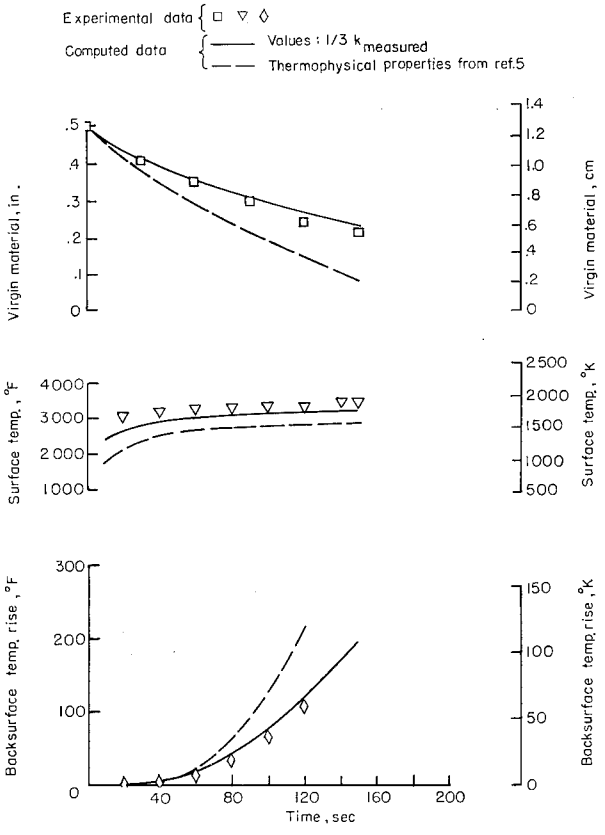

Figure 18.- Comparison of experimental recession and temperature histories with computer program outputs for PN-1.

The measured thermophysical properties were used in the first computation and the resulting thermal response is compared with the experimental results in figures 18 and 19. The experimental data are shown as symbols and the computed data are shown as dashed lines. As can be seen, the measured thermophysical properties did not produce a close comparison with the experimental results.

When the measured thermal conductivity of the char was reduced by one-third, a relatively good comparison was achieved, as is shown in figures 18 and 19 by the solid lines.

An emissivity of 1.0 was used in calculating the surface temperatures for PN-1 and PN-2. The use of the measured values of emissivity for PN-1 and PN-2 from reference 5 would have resulted in an experimental surface temperature less than 3 percent higher than the temperatures plotted in figures 18 and 19. This would have resulted

in a wider difference in the experimental and computed surface temperatures but would not be observable on the scale of figures 18 and 19.

This exercise indicates that the values of char thermal conductivities are too large by roughly a factor of three and corroborates an observation advanced in reference 27, although not exactly of the same magnitude.

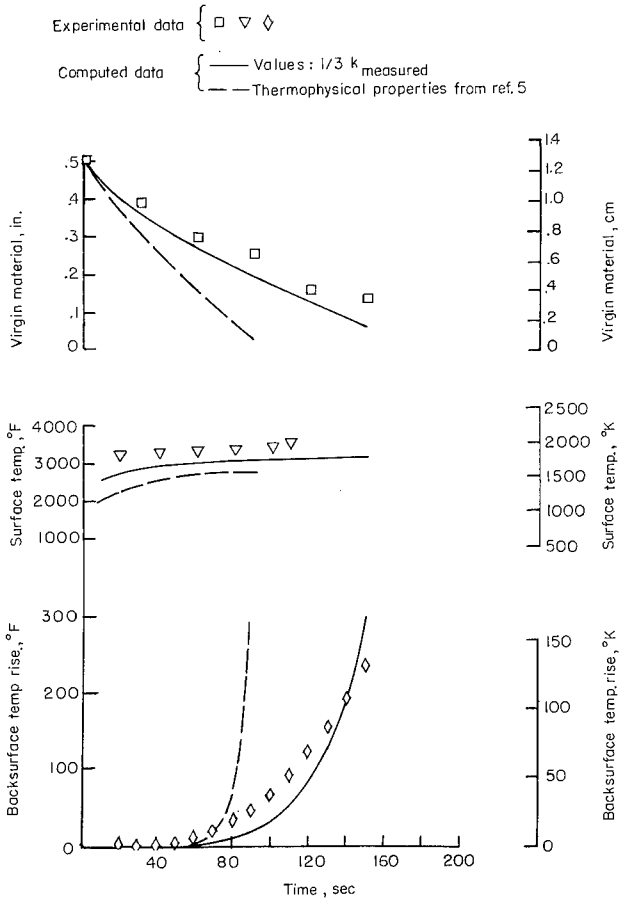

Figure 19.- Comparison of experimental recession and temperature histories with computer program outputs for PN-2.

SUMMARY OF RESULTS

Five phenolic-nylon-based materials have been tested in a supersonic airstream ($M \approx 5$) at an enthalpy of 4800 Btu/lb (11.16 MJ/kg). The pressure and heat-transfer rate at the stagnation point of the model were 0.066 atmosphere and 119 Btu/ft^2-sec $\left(1.35 \frac{MW}{m^2}\right)$, respectively. The test facility was found to provide consistent test conditions. Measured distributions of heating rate and pressure were found to be in good agreement with theoretical predictions and measurements obtained from other hypersonic wind tunnels, thus indicating a smooth, uniform flow stream. The shear level in this environment was low and, as expected, all char removal during the present tests was due entirely to oxidation. The experimental data obtained have been analyzed and compared with available theoretical predictions. The results of these analyses and comparisons may be summarized as follows:

1. For the data obtained in the present investigation reasonable agreement between calculated and measured char-recession rates was obtained by assuming chemical equilibrium at the char surface. When the pyrolysis gases were assumed inert and CO was specified as the principal reaction product, the calculated char-recession rates exceeded the measured rates by a factor of approximately 2.

2. In high-density materials, the addition of 12.5 percent (by weight) of silica resulted in a 20-percent decrease in thermal effectiveness; however, a significant increase in both char integrity and char-virgin-material interface strength was produced.

3. The SiO_2-C reactions did not significantly affect the char-recession rates observed in the present tests.

4. From a series of computer calculations for the materials PN-1 and PN-2, it was found that no simultaneous agreement between measured and calculated char surface temperature, pyrolysis interface locations, and back surface temperature rise could be obtained, when measured thermophysical properties from NASA TN D-2991 were used in the ablation computer program described in NASA TN D-2076. However, when the char thermal conductivities were reduced by approximately one-third, reasonable agreement between computer calculations and measured material response was obtained.

Langley Research Center,
National Aeronautics and Space Administration,
Langley Station, Hampton, Va., September 12, 1967,
124-08-03-05-23.

APPENDIX

DETERMINATION OF VIRGIN-MATERIAL AND CHAR DENSITIES

Four of the phenolic-nylon-based materials were subjected to decomposition in a vacuum oven to obtain sufficient char for density measurements. (Virgin-material densities were determined also during this analysis.)

Shrinkage of Char

Consider the element of ablation material, xyz, shown in sketch 1.

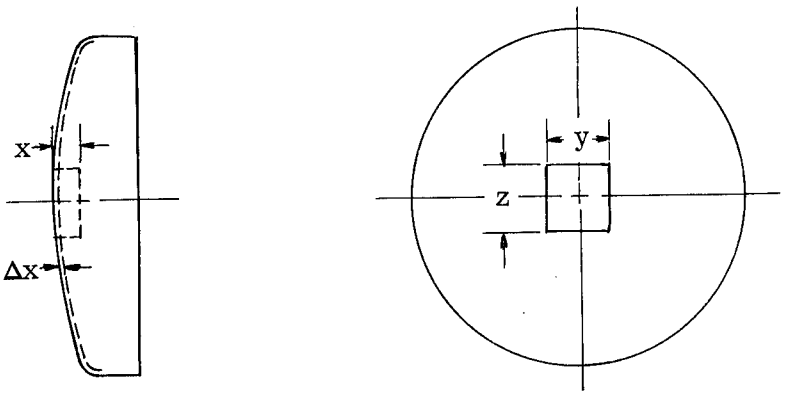

Sketch 1

When the material in this volume element chars, it shrinks. This shrinkage causes a change in the dimension of the element perpendicular to the char surface. This change is shown in sketch 1 as Δx. In the yz-plane, the shrinkage does not cause a change in the dimensions of the element. Instead, the shrinkage causes the fissures previously shown in figure 9. Hence, the volume of the element shown in sketch 1, prior to the shrinkage, is

$$V = xyz$$

and the volume after shrinkage is

$$V' = yz(x - \Delta x)$$

$$\frac{V'}{V} = 1 - \frac{\Delta x}{x}$$

Accordingly, the ratio of the char density based on initial dimensions, ρ_c^o, to the char density based on dimensions after shrinkage, ρ_c is

$$\frac{\rho_c^o}{\rho_c} = 1 - \frac{\Delta x}{x}$$

APPENDIX

Experimental Procedure

Small rectangular prisms of each of the materials used in this test program (except PN-1) were accurately weighed and the distance between parallel faces was measured before the specimens were placed in the oven. (See table AI.) Duplicate determinations were made in each case. After the specimens were placed inside, the oven was sealed, purged with nitrogen, and evacuated. The oven was held at 623° K for 18 hours and 823° K for four hours. Pressure inside the oven ranged from 0.53×10^{-7} to 1.32×10^{-7} atm. After cooling, the charred specimens were removed, weighed, and the distance between parallel faces measured again.

All the measurements made on the density-determination specimen are recorded in table AI. The reasoning as to the shrinkage of the char in one dimension, as explained earlier in this appendix, was applied to specimens charred in the oven. An average value of the change in length per unit length was determined from the measurement data, and the char-density correction factor $\frac{1}{1 - \frac{\Delta x}{x}}$ was computed. The weight of SiO_2 remaining in the oven specimen was subtracted and a density value was calculated. This value of char density was subtracted and another density value was calculated. This second value of char density was needed for the theoretical char oxidation analysis and represents the density of the reactive material available in the char layer. Since a small amount of unreactable residue (determined from the elemental analysis) was found in PN-2, a slight correction was applied to this material's char specific gravity in the manner just described. This correction was to insure that the specific gravities of the chars as determined herein would be consistent with the elemental analysis of the actual formulation. The specific gravities of the virgin material, the char containing SiO_2, and the char with SiO_2 excluded are listed in table AI, as well as in table I of the main text.

TABLE AI.- WEIGHT AND LENGTH MEASUREMENTS BEFORE AND AFTER DECOMPOSITION AND COMPUTED SPECIFIC GRAVITIES

Material	Decomposition	Specimen dimension			$\frac{1}{1 - \frac{\Delta x}{x}}$	Weight, grams	Weight percent after SiO_2 subtracted	Specific gravity		
		y, cm	z, cm	x, cm				Virgin material	Char including SiO_2	Char excluding SiO_2
PN-2	Before	0.907	0.907	1.905	1.128	1.1087	-----	0.707	0.243	0.234
	After	.810	.802	1.678		.3379	0.3252			
PN-4	Before	1.173	1.174	2.527	1.128	2.0111	-----	0.576	0.163	0.130
	After	1.040	1.039	2.253		.5053	0.4025			
PNS-5	Before	1.216	1.213	1.216	1.071	2.2214	-----	1.233	0.401	0.337
	After	1.148	1.150	1.109		.6742	0.5672			
PNS-12	Before	1.201	1.201	1.201	1.046	2.2286	-----	1.280	0.510	0.347
	After	1.171	1.164	1.112		.8500	0.5792			

REFERENCES

1. Hiester, Nevin K.; and Clark, Carroll F.: Feasibility of Standard Evaluation Procedures for Ablating Materials. NASA CR-379, 1966.

2. Vojvodich, Nick S.; and Winkler, Ernest L.: The Influence of Heating Rate and Test Stream Oxygen Content on the Insulation Efficiency of Charring Materials. NASA TN D-1889, 1963.

3. Chapman, Andrew J.: Effect of Weight, Density, and Heat Load on Thermal-Shielding Performance of Phenolic Nylon. NASA TN D-2196, 1964.

4. Mechtly, E. A.: The International System of Units – Physical Constants and Conversion Factors. NASA SP-7012, 1964.

5. Wilson, R. Gale, compiler: Thermophysical Properties of Six Charring Ablators From 140° to 700° K and Two Chars From 800° K to 3000° K. NASA TN D-2991, 1965.

6. Schaefer, William T., Jr.: Characteristics of Major Active Wind Tunnels at the Langley Research Center. NASA TM X-1130, 1965.

7. Exton, Reginald J.: Theory and Operation of a Variable Exposure Photographic Pyrometer Over the Temperature Range 1800° to 3600° F (1255° to 2255° K). NASA TN D-2660, 1965.

8. Holloway, Paul F.; and Dunavant, James C.: Heat-Transfer and Pressure Distributions at Mach Numbers of 6.0 and 9.6 Over Two Reentry Configurations for the Five-Stage Scout Vehicle. NASA TN D-1790, 1963.

9. Cohen, Nathaniel B.: Boundary-Layer Similar Solutions and Correlation Equations for Laminar Heat-Transfer Distribution in Equilibrium Air at Velocities up to 41,100 Feet Per Second. NASA TR R-118, 1961.

10. Smith, A. M. O.; and Clutter, Darwin W.: Machine Calculation of Compressible Laminar Boundary Layers. AIAA J., vol. 3, no. 4, Apr. 1965, pp. 639-647.

11. Dow, Marvin B.; Pittman, Claud M.; and Croswell, William F.: Thermal Performance and Radio-Frequency Transmissivity of Several Ablation Materials. NASA TN D-1896, 1964.

12. Scala, Sinclaire M.: The Ablation of Graphite in Dissociated Air, Part I: Theory. R62SD72, Missile and Space Div., Gen. Elec. Co., Sept. 1962.

13. Moore, Jeffrey A.; and Zlotnick, Martin: Combustion of Carbon in an Air Stream. ARS J., vol. 31, no. 10, Oct. 1961, pp. 1388-1397.

14. Parker, Almon S.; and Hottell, H. C.: Combustion Rate of Carbon. Study of Gas-Film Structure by Microsampling. Ind. Eng. Chem., vol. 28, no. 11, Nov. 1936, pp. 1334-1341.

15. Gulbransen, Earl A.; and Andrew, Kenneth F.: Reactions of Artificial Graphite: Kinetics of Oxidation of Artificial Graphite at Temperatures of 425° to 575° C and Pressures of 0.15 to 9.8 cm. of Mercury of Oxygen. Ind. Eng. Chem., vol. 44, no. 5, May 1952, pp. 1034-1044.

16. Byholder, George; and Eyring, Henry: Kinetics of Graphite Oxidation. J. Chem. Phys., vol. 61, no. 5, May 1957, pp. 682-688.

17. Scala, Sinclaire M.; and Gilbert, L. M.: The Sublimation of Graphite at Hypersonic Speeds. R64SD55 (Contracts No. 04(647)-269 and AF 04(694)-222), Missile and Space Div., Gen. Elec. Co., Aug. 1964.

18. Diaconis, N. S.; Gorsuch, P. D.; and Sheridan, R. A.: The Ablation of Graphite in Dissociated Air – Part II: Experiment. IAS Paper No. 62-155, June 1962.

19. Metzger, J. W.; Engel, M. J.; and Diaconis, N. S.: The Oxidation and Sublimation of Graphite in Simulated Re-entry Environments. AIAA Paper No. 65-643, Sept. 1965.

20. Beecher, Norman; and Rosensweig, Ronald E.: Ablation Mechanisms in Plastics With Inorganic Reinforcement. ARS J., vol. 31, no. 4, Apr. 1961, pp. 532-539.

21. Blumenthal, Jack L.; Santy, Myrrl J.; and Bruns, Eugene A.: Kinetic Studies of High-Temperature Carbon-Silica Reactions in Charred Silica-Reinforced Phenolic Resins. AIAA J., vol. 4, no. 6, June 1966, pp. 1053-1057.

22. Walberg, Gerald D.: Analytical Study of Diffusion-Controlled Char Oxidation and Its Effect on Steady-State Ablation of Plastic Materials. NASA TR R-242, 1966.

23. Dow, Marvin B.; and Swann, Robert T.: Determination of Effects of Oxidation on Performance of Charring Ablators. NASA TR R-196, 1964.

24. Swann, Robert T.; Pittman, Claud M.; and Smith, James C.: One-Dimensional Numerical Analysis of the Transient Response of Thermal Protection Systems. NASA TN D-2976, 1965.

25. Kotanchik, Joseph N.; and Erb, R. Bryan: The Design of Ablative Thermal Protection Systems. Paper presented 7th International Aeronautical Congress (Paris, France), June 1965.

26. Strouhal, G.; Curry, D. M.; and Janney, J. M.: Thermal Protection System Performance of the Apollo Command Module. AIAA/ASME Seventh Structures and Materials Conference, Apr. 1966, pp. 184-200.

27. Brazel, J. P.; Tanzilli, R. A.; and Begany, A. R.: Determination of the Thermal Performance of Char Under Heating Conditions Simulating Atmospheric Entry. AIAA Paper No. 65-640, Sept. 1965.

NASA-Langley, 1968 —— 18 L-5248

"The aeronautical and space activities of the United States shall be conducted so as to contribute . . . to the expansion of human knowledge of phenomena in the atmosphere and space. The Administration shall provide for the widest practicable and appropriate dissemination of information concerning its activities and the results thereof."

—NATIONAL AERONAUTICS AND SPACE ACT OF 1958

NASA SCIENTIFIC AND TECHNICAL PUBLICATIONS

TECHNICAL REPORTS: Scientific and technical information considered important, complete, and a lasting contribution to existing knowledge.

TECHNICAL NOTES: Information less broad in scope but nevertheless of importance as a contribution to existing knowledge.

TECHNICAL MEMORANDUMS: Information receiving limited distribution because of preliminary data, security classification, or other reasons.

CONTRACTOR REPORTS: Scientific and technical information generated under a NASA contract or grant and considered an important contribution to existing knowledge.

TECHNICAL TRANSLATIONS: Information published in a foreign language considered to merit NASA distribution in English.

SPECIAL PUBLICATIONS: Information derived from or of value to NASA activities. Publications include conference proceedings, monographs, data compilations, handbooks, sourcebooks, and special bibliographies.

TECHNOLOGY UTILIZATION PUBLICATIONS: Information on technology used by NASA that may be of particular interest in commercial and other non-aerospace applications. Publications include Tech Briefs, Technology Utilization Reports and Notes, and Technology Surveys.

Details on the availability of these publications may be obtained from:

SCIENTIFIC AND TECHNICAL INFORMATION DIVISION

NATIONAL AERONAUTICS AND SPACE ADMINISTRATION

Washington, D.C. 20546